Heliyon 7 (2021) e08089

Contents lists available at ScienceDirect

Heliyon

journal homepage: www.cell.com/heliyon

Research article

Targeting cathepsins: A potential link between COVID-19 and associated neurological manifestations

Kartikay Prasad [a,1], Shahzaib Ahamad [b,1], Dinesh Gupta [b,**], Vijay Kumar [a,*]

[a] Amity Institute of Neuropsychology & Neurosciences, Amity University, Noida, UP, 201303, India
[b] Translational Bioinformatics Group, International Centre for Genetic Engineering and Biotechnology (ICGEB), Aruna Asaf Ali Marg, New Delhi 110067, India

ARTICLE INFO

Keywords:
COVID-19
SARS-CoV-2
Cathepsins
Neurological manifestations
Drug repurposing
Cyclosporine

ABSTRACT

Many studies have shown that the lysosomal cathepsins, especially cathepsins B/L (CTSB/L) are required for SARS-CoV-2 entry into host cells. Lysosomal proteases, cathepsins are indispensable for normal health and are involved in several brain disorders occurring at different development age periods. On the other hand, it has been well known that COVID-19 infection is largely associated with several neurological disorders. Taken together these findings and given the high levels of expression of CTSB/L in the brain, we here proposed a reasonable hypothesis about the involvement of CTSB/L in the neurological manifestations linked to COVID-19. Pharmacological inhibitions of the CTSB/L could be a potential therapeutic target to block the virus entry as well as to mitigate the brain disorders. To this end, we utilized the network-based drug repurposing analyses to identify the possible drugs that can target CTSB/L. This study identifies the molecules like cyclosporine, phenytoin, and paclitaxel as potential drugs with binding ability to the CTSB/L. Further, we have performed molecular docking and all-atom molecular dynamics (MD) simulations to investigate the stability of CTSL-drug complexes. The results showed strong and stable binding of drugs with CTSL.

1. Introduction

The spread of a novel coronavirus, severe acute respiratory syndrome (SARS-CoV-2) is disrupting the global health and economy (Li et al., 2020). As of July 2021, over 180 million confirmed cases are reported worldwide with more than 4.0 million deaths reported (https://covid19.who.int/). There are more than two-thousand on-going clinical trials underway, but to date, none of these drugs have proven clinically-effective.

SARS-CoV-2 enters the host cell through spike (S) protein which binds to angiotensin-converting enzyme 2 (ACE2) receptor present on the cell-membrane of host cells (Zhou et al., 2020b). This binding is then followed by the cleavage of the S protein by the host transmembrane serine protease 2 (TMPRSS2) and then fusion to the host cell membrane (Hoffmann et al., 2020). However studies have indicated the involvement of the endosomal pathway as the key entry for SARS-CoV (Millet and Whittaker, 2015; Wang et al., 2008). These studies showed that the virus enters the host cell via a pH- and receptor-mediated endocytosis pathway. In this pathway, the lysosomal cathepsins, mainly cathepsin L (CTSL) and cathepsin B (CTSB) cleaves and activate the S protein which then fuses with host cells (Ou et al., 2020; Zhou et al., 2015). An additional receptor for the S protein has been recognized as CD147 through in vitro experiment (Wang et al., 2020). Interestingly, both CTSL and CD147 are largely present in the central nervous system (CNS) (Hook et al., 2020; Podvin et al., 2018) whereas TMPRSS2 is poorly present in the brain (Paoloni-Giacobino et al., 1997).

While COVID-19 is known to cause substantial respiratory pathology including pneumonia and acute respiratory distress syndrome (ARDS), increasing clinical evidence points to the presence of several neurological manifestations (Ellul et al., 2020; Gupta et al., 2020a; Khatoon et al., 2020, 2021; Leonardi et al., 2020). These symptoms include headache, dizziness, weakened consciousness, ataxia, acute cerebrovascular disease, and epilepsy predominantly in the CNS. Moreover, symptoms like hypogeusia, hyposmia, and neuralgia are prevalent in the peripheral nervous system (PNS) along with different musculoskeletal symptoms (Mao et al., 2020). Also, acute encephalopathy (Filatov et al., 2020) and acute hemorrhagic necrotizing encephalopathy (ANE) (Poyiadji et al., 2020) have been reported in several case report studies. Acute

* Corresponding author.
** Corresponding author.
E-mail addresses: dinesh@icgeb.res.in (D. Gupta), vkumar33@amity.edu (V. Kumar).
[1] Contributed equally.

https://doi.org/10.1016/j.heliyon.2021.e08089
Received 9 February 2021; Received in revised form 21 April 2021; Accepted 26 September 2021

inflammatory demyelinating polyneuropathy (Guillain-Barré syndrome) has also been reported in some COVID-19 patients (Toscano et al., 2020). A very recent study presented neurochemical evidence of neuronal injury and glial activation in COVID-19 patients (Kanberg et al., 2020).

The potential mechanisms underpinning the various neurological syndromes include direct or indirect viral neuronal injury (Zubair et al., 2020), a secondary hyper inflammation syndrome related to cytokine storm (Mehta et al., 2020), post-infectious immune-mediated disorders, or the effects of a severe systemic disorder with the neurological consequences of sepsis, hyperpyrexia, hypoxia, vasculopathy and/or coagulopathy (Bhimaneni et al., 2021; Sau and Kumar, 2021). However, the presence of SARS-CoV-2 in the brain is still doubtful and there is no evidence to date in either animal or human studies. Though, some studies have shown the presence of SARS-CoV in the CNS and cerebrospinal fluid (CSF) (Hung et al., 2003; Xu et al., 2005; Zhou et al., 2020a) or brain parenchyma of patients (Paniz-Mondolfi et al., 2020). Moreover, some clinical studies on SARS-CoV patients have reported the presence of virus particles in the neurons of the brain (Gu et al., 2005; Khatoon et al., 2020). Understanding the molecular mechanisms behind the increased risk for neurological disorders in COVID-19 patients would provide clues toward their pathophysiology and the identification of therapeutic targets.

The abundant expression of cathepsins in the human brain at all ages and throughout the brain suggests the involvement of normal lysosomal functions and in neurological disorders. Intriguingly, cathepsin L and cathepsin B is abundantly expressed in hippocampal and cortical regions of the human brain which are largely involved in cognitive and behavioral functions.

Having all these pieces of information together and looking into the urgent calls for treatments of the current global pandemic of COVID-19, we suggest here that cathepsins B/L (CTSB/L) might be implicated in neurological disorders associated with COVID-19 and targeting these cathepsins will be a more promising approach for COVID-19 to mitigate the risks of neurological consequences. Given that the extent of the burden of neurological disease associated with COVID-19 pandemic, we support a unified approach of the treatment of COVID-19 patients.

In this study, we report a network-based biological framework to demonstrate the molecular interplay between (CTSB/L) and different brain disorders associated with COVID-19. Furthermore, we utilized the network-based drug repurposing and extensive computational approach similar to our previous studies (Prasad et al., 2020, 2021a) to identify the possible drugs targeting CTSB/L. We report cyclosporine A (CsA), phenytoin, and paclitaxel as putative drugs that interacts with CTSB/L and thus could be considered as a candidate drug for repurposing. We next performed molecular docking and all-atom molecular dynamics (MD) simulations to explore the binding of the three drugs to CTSL and investigate the interaction mechanisms in detail. These results indicate strong and stable interactions of the drugs with CTSL, suggesting a promising therapeutic intervention for COVID-19.

2. Methods

2.1. Gene-gene and gene-drug interactions network

A list of 332 human genes known to interact with SAR-COV2 viral proteins reported by Gordon et al. (2020) was retrieved. For identifying the COVID-19 target genes showing interaction with CTSB/L, first we have retrieved the list of genes interacting with CTSB/L and then identify genes directly interacting with CTSB/L and were also interacting with SARS-CoV-2 protein. Further, a functional enrichment analysis of this interaction network was studied by Genemania web server (Zuberi et al., 2013). In the next step, we have identified the neurological diseases associated with the identified genes. For identifying the neurological disease associated with the genes, several databases such as Genecard (Stelzer et al., 2016), OMIM (Amberger et al., 2019), MalaCards (Rappaport et al., 2017), CTD (Davis et al., 2019), and PubChem (Kim et al., 2019) along with literature were searched extensively. Cytoscape tool was used for creating the disease-gene interaction network (Shannon et al., 2003).

Further, for drug repurposing of CTSB/L, multiple drug-gene interaction databases such as DrugBank, DGIdb and Pubchem (Cotto et al., 2018; Kim et al., 2021; Wishart et al., 2008) were searched and a total of 71 drugs were identified for CTSB/L genes. STITCH database (Kuhn et al., 2007) was used for preparing the drug-gene interaction network. STITCH is a database known to predict the physical and functional interaction between the query genes and drugs. The interactions in the STITCH database are derived from five sources namely, automated text mining, high throughput lab experiment data, co-expression interaction data, interaction prediction by genomic context, and by previous knowledge from other databases. For each interaction, STITCH calculated a combined score. A combined score is calculated by combining the corrected probability of observing an interaction randomly and probabilities of interaction from different evidence channels. A drug-gene interaction was considered significant if the combined score was greater than 0.7.

2.2. Molecular docking

The mol file of phenytoin and cyclosporin was downloaded from Drug Bank. The structure of CTSB (PDB: 1HUC) and CTSL (PDB:4AXL) was downloaded from the RCSB protein data bank (Berman et al., 2000). Energy minimization of both the target molecules was done using the Swiss-PDB viewer (Guex and Peitsch, 1997) to obtain the stable and lowest energy conformation state of the proteins. The structures of CTSB/L were prepared for docking by adding Kollman charges and hydrogen atoms to the polar groups of the protein using AutoDock tools (Morris et al., 2009). AutoDock Vina (Trott and Olson, 2010) was used for docking the identified drugs to the target molecules. The blind docking and screening were performed for the drugs (Gupta et al., 2018, 2020b). The grid spacing was set to 1 Å and exhaustiveness was 8. A system with i5 processor with 12 GB of RAM was used for molecular docking experiment.

2.3. Molecular dynamics (MD) simulation

MD simulations were carried out by GROMACSv5.18.3 software package. The three-dimensional (3D) structure of native CTSL was collected from PDB database. The determination of charge states for the ionizable residues was performed using H^{++} calculation to understand protonation state of the protein (Gordon et al., 2005). Due to the lack of suitable force field parameters for drug like molecules in the GROMACS software, PRODRG server was used for generation of molecular topologies and coordinate files (Scattelkopf and Van Aalten, 2004). The native and complexes topology parameter files were created out by the CHARMM27 force field included with CMAP correction (Vanommeslaeghe et al., 2010). The intermolecular (non-bonded) potentials, Lennard–Jones (LJ) potential with a cut-off distance range of 8 to 10Å, pairwise Coulomb interaction and the long-range electrostatic force were determined by particle mesh Ewald(PME) approach (Lee et al., 2016) with the cut-off set to 1.2 nm (Wang et al., 2016). The system was then immersed with the TIP3P water model, and the protein was placed at the center of the cubic grid box (1.0 nm^3) (Price and Brooks, 2004). To neutralize system 0.15 M counter ions (Na^+ and Cl^-) were added (Joung and Cheatham, 2008). The neutralized system was then subjected to energy minimization using the Steepest Descent (SD) and Conjugate Gradient (CG) algorithms utilizing a convergence criterion of 0.005 kcal mol^{-1} $Å^{-1}$. The equilibration phase was carried out separately for 500 ps in NVT (atom, volume, temperature) and NPT (atom, pressure-temperature) for each system. LINear Constraint Solver (LINCS) algorithm was used to constrain the bonds and angles (Berk et al., 1997). Nosé-Hoover thermostat and Parinello–Rahman barostat was then applied to maintain the temperature and the pressure of the system, respectively. The system was maintained constant at 1 bar and 300 K,

with a coupling time of τP = 2 ps, and τT = .1 ps, respectively. Finally, using the NPT ensemble, production runs were performed for the period of 100 ns, with time integration. The energy, velocity, and trajectory were updated at the time interval of 10 ps.

Gromacs utilities and python scripts with MDTraj (McGibbon et al., 2015) were used to analyze the global structural order parameters, i.e., RMSD (root mean square deviation), Rg (radius of gyration), SASA (solvent accessible surface area), RMSF (root mean square fluctuation), PCA (Principal component analysis), free energy landscape (FEL). DSSP were used to investigate the secondary structure conformational dynamics during the MD simulation (Kabsch and Sander, 1983). The energy plots and graphs were marked and visualized using QtGrace visualization tool.

2.3.1. Principal component analysis (PCA) and free-energy landscape

The principal component analysis (PCA) determines the motion information in MD simulations that can be correlated to biological function (Abdi and Williams, 2010; Sang et al., 2017). The eigenvalues were determined by diagonalizing the matrix with their projection along with the first two principal components (PC1and PC2) and were calculated using essential dynamics (ED) method by g_covar, g_anaeig modules.

PC1 and PC2 were then selected as reaction coordinates for the calculation of free energy, Gα using:

$$G\alpha = -kT \ln[(q\alpha)\, Pmax(q)]$$

where, k is the Boltzmann constant, T is the simulation temperature. P(qα) represents the probability density function and was constructed using a joint probability distribution of reaction coordinates (PC1 and PC2). Pmax(q) represents the probability of the most probable state.

3. Results and discussion

3.1. Network-based gene-gene and gene-drug interactions

A list of 332 human target genes of SARS-CoV-2 was retrieved from Gordan et al. (Gordon et al., 2020). From this virus-host interactome study, we have identified four human target genes namely CRTC3, NPC2, IDE, and RAB7A which interact with CTSB and CTSL (Supporting Information Figure S1). Further, biological process enrichment analysis of these six genes using GeneMania webserver indicated their role in endopeptidase activity, antigen processing and presentation of peptide or polysaccharide antigen, activation of innate immune response, extracellular matrix organization, and positive regulation of defense response (Figure 1 and Supporting information Table 1).

A disease-gene interaction network was then constructed as described in the methods section. A disease-gene interaction map of the six candidate genes was constructed from the disease-gene interaction data of the brain obtained from various databases. A total of 69 disease-gene interactions were obtained linking these 6 genes with 59 different brain-related disorders (Figure 2 and Supporting information Table 2). Moreover, to demonstrate the association between COVID-19 and brain disorders, a disease-disease association network was constructed as described previously (Prasad et al., 2021a), where we have identified 28 neurological diseases directly linked with COVID-19. Several diseases like ataxia, dysarthria, spasticity, cerebral atrophy, autism, dementia, and stroke were closely related to the COVID-19 and are also connected with multiple genes in the brain. We have identified some common neurological disorders such as Dementia, Autism, Parkinson's disease, Amyotrophic Lateral Sclerosis, Cerebral aneurysm, Encephalopathy, Meningitis, and dystonia linked with COVID-19 (Figure 2). CTSB has a role in Parkinson's disease, cerebral and brain aneurysm, brain meningitis which shows interaction with COVID-19, and is also reported in COVID-19 positive cases. Genes such as NPC2, RAB7A, IDE, CRTC3, and CTSL are also linked with the disease which is most directly and indirectly linked with COVID-19. Interestingly, recent studies showed that expression levels of CTSL, CTSB along with ACE2, and TMPRSS2, were upregulated in aged human cardiomyocytes (Emma L. Robinson et al., 2020), and in human airway epithelial cells (Yin et al., 2020).

Next, we have identified drugs against CTS B/L genes by screening multiple databases related to drug-genes interaction (Cotto et al., 2018; Davis et al., 2019; Wishart et al., 2018). For CTSB, 10 significant interactions were identified and for CTSL, 4 significant interactions were identified in the STITCH database (Figure 3 and Supporting information Table 3). Out of these drugs, cyclosporine A (CsA) and phenytoin were commonly interacting with both CTSB and CTSL genes. Given that CTSB/L are critical for the SARS-CoV-2 entry and are largely involved in

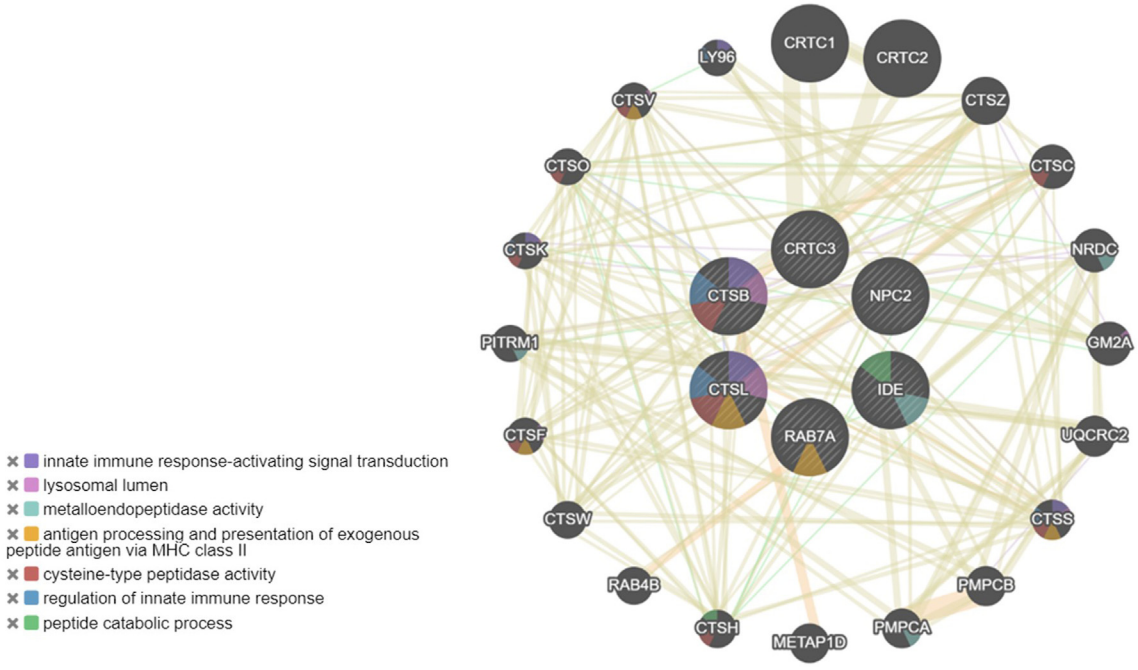

Figure 1. Enrichment analysis of cathepsin interacting genes. Gene network of cathepsin interacting genes derived from GeneMANIA along with functional enrichment.

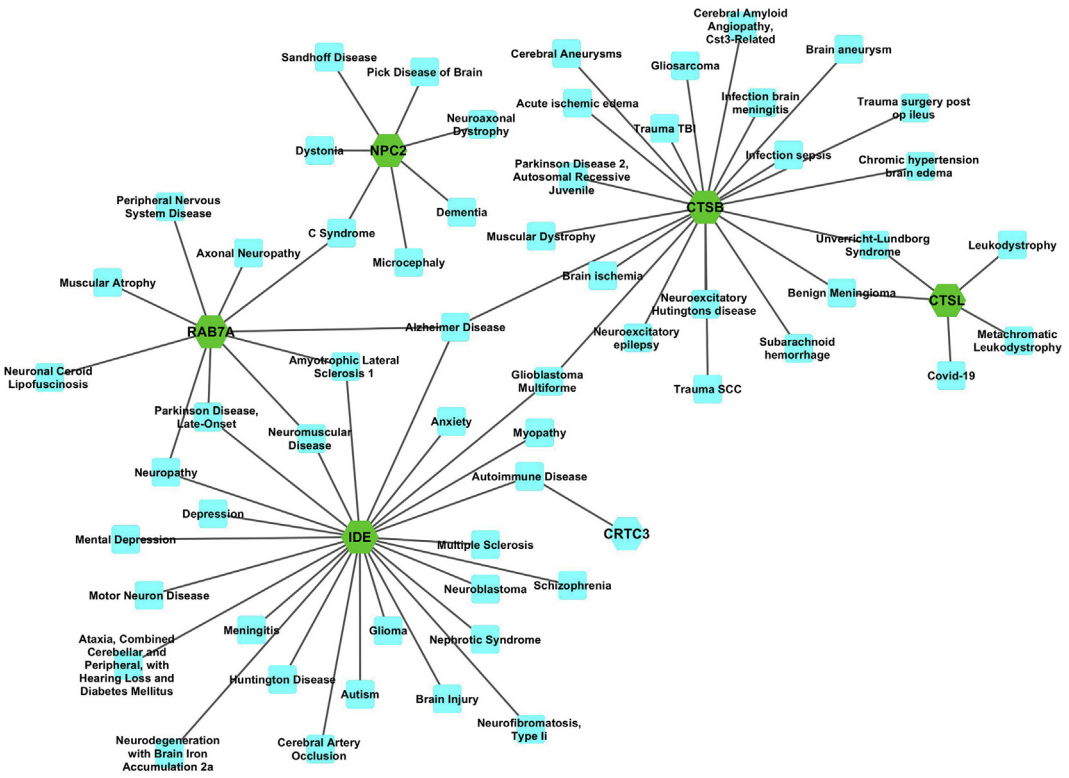

Figure 2. Disease gene interaction network. The figure represents the interaction of cathepsins and cathepsin target genes (Circled in green) with their related brain disorder represented by blue colors.

causing brain disorders, inhibition of these proteases through a single drug molecule could be a compelling strategy for the treatment of COVID-19 and neurological manifestations of COVID-19 as well.

3.2. Molecular docking analysis

All the drugs studied were docked against the three-dimensional structures of CTSB and CTSL and were ranked based on their binding affinity and the maximum number of interactions with the target residues (Table 1). The binding energy suggests that these drugs bind with the CTD with a strong affinity with K_D ($K_D = \exp^{\Delta G/RT}$) values in the nanomolar to low micromolar range.

Among the drugs, CsA binds to CTSB and CTSL with the binding affinity of -6.8 kcal/mol and -6.5 kcal/mol, respectively. For CTSB, CsA forms a single hydrogen bond with Arg153 along with nine van der Waals bonds (Figure 4A). Whereas, CsA binds to CTSL with two hydrogen bonds, Gln19 and Gly23 along with seven van der Waals bonds (Figure 4B). The three-dimensional structure of CsA-CTSB/L drug complexes indicates that the drug binds near to the active site of the molecule and the binding of CsA to CTSL also involved the active site residue Cys25, and metal-binding site, His163 (Figure 4C and D).

The other drug, phenytoin binds to CTSB with the binding affinity of -7.0 kcal/mol and forms two hydrogen bonds with Pro57 and Thr71 along with 8 van der Waals bonds (Figure 5A). It binds with CTSL with a binding affinity of -6.5 kcal/mol and forms a single hydrogen bond with Cys22, along with seven van der Waals interactions (Figure 5B). Structurally, phenytoin binds to CTSB at the N-terminal large loop region (Figure 5C), whereas phenytoin binds to CTSL in the N-terminal loop structure and also includes the ligand-binding residue Leu144, and metal-binding residue, His163 (Figure 5D).

Furthermore, we also identified another drug, Paclitaxel which binds to CTSL with a much stronger affinity than the other two drugs. It binds to CTSL with -7.7 kcal/mol of binding affinity and forms a single hydrogen bond with Trp189 along with ten van der Waals interactions, explaining its strong affinity (Figure 6A). The structure of the drug-protein complex also showed the involvement of the N-terminal loop along with C-terminal ligand-binding residues, His163, Trp189, and Glu192 (Figure 6B). Thus, the overall results of molecular docking suggest the strong binding of the drugs to CTSL will disrupt the active site as well as the metal-binding site, and thus could inhibit the protein.

3.3. Molecular dynamics simulation analysis

The structural stability of the CTSL-drug complexes was assessed using the Cα-RMSD of the backbone atoms relative to the protein. The RMSD describes the measure of the changes in the conformation of a given structure over time. The apo CTSL showed fluctuations throughout the 100 ns simulation with the RMSD values of ~0.2 nm–~0.4 nm (Figure 7A). The RMSD of apo CTSL remained less to the CTSL-drug complexes till ~70 ns and then increased. The ctsl-drug complexes underwent conformational fluctuation at different RMSD levels till ~70 ns, and they equilibrated afterward. Among the drugs, CTSL-CsA complex has higher RMSD till ~70 ns and then remains stable with an RMSD value of ~0.3 nm, with a maximum RMSD of ~0.35 nm (Figure 7A). The CTSL-phenytoin complex has lowest RMSD with the mean RMSD value of ~0.25 nm indicating that phenytoin binds stably with CTSL during the simulation. This shows that the three drugs maintained stable binding with the CTSL towards the end of the simulation.

The stability of a protein can also be estimated using *Rg* analysis, which describes the compactness of the protein. The CTSL-drug complexes showed lower *Rg* deviations than apo CTSL and became lower and more stable during the last ~40 ns of simulation (Figure 7B). Also, the *Rg* value of CTSL in complex with phenytoin showed more fluctuations and became stable at the end of the simulation with the lowest *Rg* value. This further showed that CTSL gained more stability upon binding to drugs.

We next analysed SASA to characterize the regions of CTSL that are accessible to solvent molecules. The SASA trajectory indicated that apo CTSL and CTSL-drug complexes maintained comparable SASA patterns

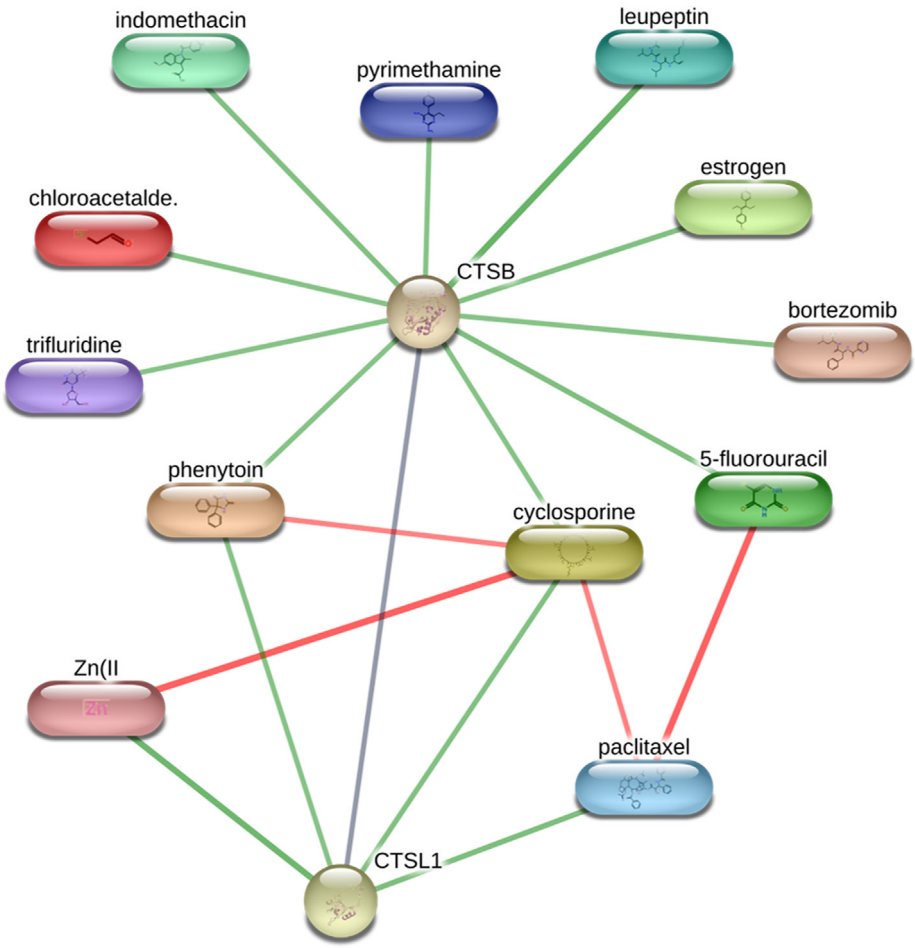

Figure 3. Drug-gene network of CTSB and CTSL using the STITCH database. The network shows that Cyclosporine and Phenytoin binds both CTSB and CTSL genes and thus could be considered as a candidate for drug repurposing.

throughout the simulation time (Figure 7C). The decrease in SASA during the last 50 ns simulation was observed for CTSL-phenytoin complex indicating the most stable complex.

The RMSF analysis of the CTSL-drug complexes in relation to apo CTSL was done to compare the dynamics of the individual residues of the protein (Figure 7D). The drug-binding residues showed lesser fluctuations whereas the flexible loop regions showed the maximum fluctuations. The drug binding to CTSL decreased the RMSF significantly at N-terminal 10–25 residues, 120–125 residue positions, and at C-terminal ~212–220 residues. For CTSL-phenytoin complex, the increase in RMSF was observed at residues ~62–65, 105–120, 174–178, and 202–206, while the decrease in RMSF value was observed at ~120–150, and 187–195 residue positions. As for CTSL-paclitaxel, increase in RMSF was observed at residues ~138–150 whereas, residues at~72–80, and at 110–130 showed significant decrease in fluctuation. The CTSL-CsA complex had overall smaller fluctuations as compared to other two drug-complexes (Figure 7D). Overall, the RMSF analysis demonstrated higher residual fluctuations from ~60-150 residues while lesser fluctuation towards the C-terminal region of the protein where the catalytic and active site residues are largely located. The results of MD analysis are also provided as raw data in supplementary files.

The protein-ligand interactions are transient and hydrogen (H) bonds play crucial role in the stability of protein-ligand complex. The trajectory of H- bond formation has been monitored during the simulation and shown in Supporting information Figure S2. The average number of H-bonds observed for CTSL-CsA and CTSL-phenytion complexes was 0–3 while, the average number of H-bonds is greater in case of CTSL-paclitaxel system, indicating the most stable binding.

Table 1. Molecular docking results of Cathepsins B/L inhibitors.

Protein-Drug	Affinity Binding (kcal/mol)	Inhibition Constant (K_i) (μM)	Hydrogen Bonds	Vander Wall bonds
CathepsinB-Cyclosporine	-6.8	9.94	ARG153	VAL1, SER2, VAL3, HIS96, LYS117, ASN118, GLY119, LEU155, PRO202
CathepsinL-Cyclosporine	-6.5	16.52	GLN19, GLY23	GLN21, CYS22, CYS25, ALA138, GLY139, ASP162, HIS163
CathepsinB-Phenytoin	-7.0	7.08	PRO57, THR71	TYR54, PRO58, CYS59, PRO68, GLY72, GLY74, ASP75
CathepsinL-Phenytoin	-6.5	16.52	CYS22	GLN19, GLY20, GLN21, GLY23, ALA138, LEU144, HIS163
CathepsinL-Paclitaxel	-7.7	2.16	TRP189	ASN18, GLN19, GLY20, GLN21, CYS22, ALA138, GLY139, ASP162, HIS163, GLU192

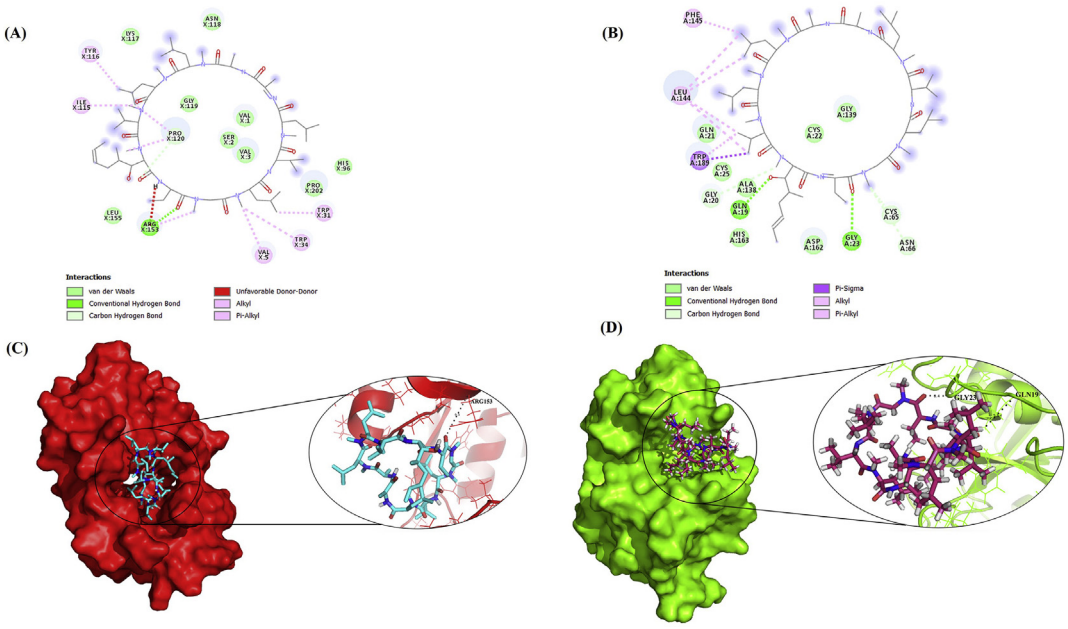

Figure 4. Molecular docking interactions of Cyclosporine to Cathepsins B/L. Two-dimensional (2D) diagrams of (A) CTSB-cyclosporine, and (B) CTSL-cyclosporine interactions using Ligplot+. The protein residues and interactions are colored accordingly and provided in figure. The potential binding poses of cyclosporine in the three-dimensional structure of the (C) CTSB, and (D) CTSL proteins. The black dotted line represents intermolecular hydrogen bond interactions.

3.4. Principal component analysis (PCA) and free energy landscape (FEL) analysis

The principal component analysis (PCA) was next used to study the significant motions during the binding of the drugs to CTSL. The conformational sampling of CTSL systems in the essential subspace is shown in Figure 8 which demonstrates the global motions along with the PC1 and PC2 projected by the Cα atom. A protein-ligand complex with stable cluster occupying less phase space in the two-dimensional (2D) projection represents a stable complex, and the complex with non-stable cluster occupying large phase space represents a less stable complex. The 2D projection of PCA clearly showed that CTSL-drug complexes occupied small conformational subspace as compared to the apo CTSL. The CTSL-CsA occupied small space than other drug complexes indicating the formation of most stable complex among all the CTSL systems. The decrease in conformational dynamics of CTSL-drug complexes may be due to a highly optimized interaction network, which restraints more effectively the backbone dynamics of the both the protein and drug.

Also, to study the effect of drugs on the conformational stability of CTSL, we have examined FEL as a function of the top two principal

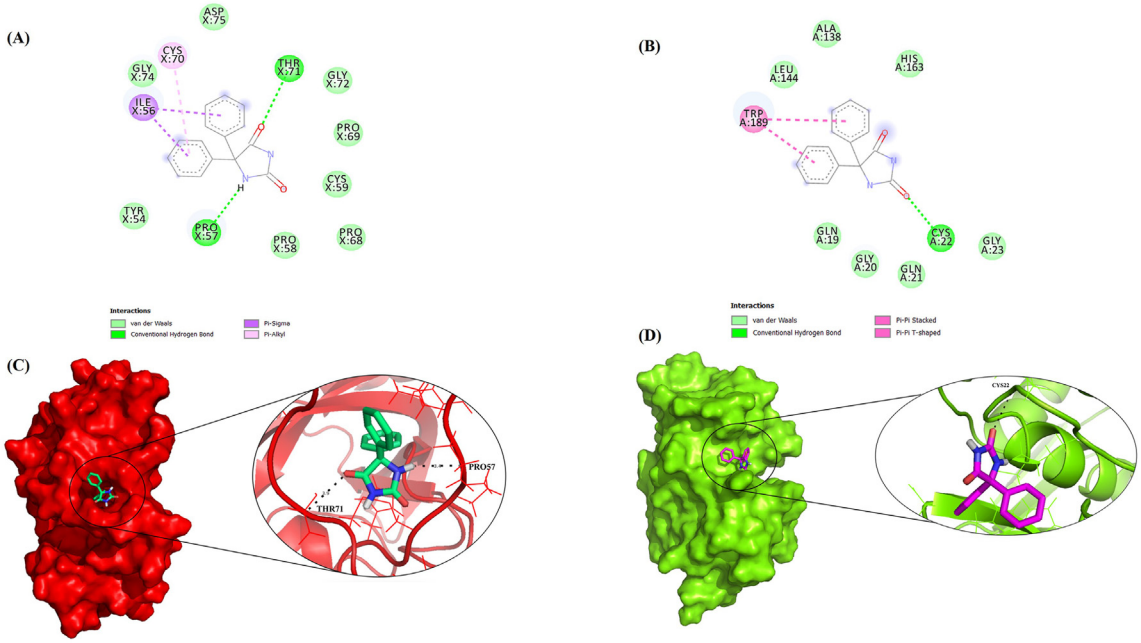

Figure 5. Molecular docking interactions of Phenytoin to Cathepsins B/L. (A) Two-dimensional (2D) diagrams of (A) CTSB-phenytoin and (B) CTSL-phenytoin interactions using Ligplot+. The description of protein residues and type of interactions are provided in figure. The potential phenytoin binding sites represented in the three-dimensional structures of the (C) CTSB, and (D) CTSL protein. The hydrogen-bond interactions are represented by a black dotted line.

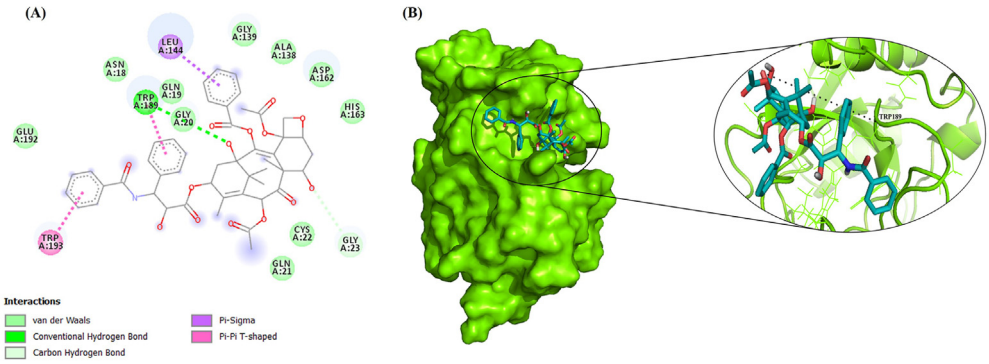

Figure 6. Molecular docking interactions of paclitaxel to CTSL. (A) Two-dimensional (2D) diagrams of protein-drug interactions using Ligplot+. (B) The potential hydrogen bond interactions and potential binding pose of paclitaxel in CTSL.

components, PC1 and PC2. FEL can be used to study the conformational redistributions induced by binding events (Kumar et al., 2018, 2019; Pandey et al., 2020; Prakash et al., 2021; Prasad et al., 2021b). Figure 9 displays the relative conformational changes of the CTSL systems where the deeper blue color indicates the lower energy and stable conformational states. As shown in the figure, FEL of apo CTSL is populated by different intermediate conformations linked by low energy barriers indicating a more relaxed and flexible protein system (Figure 9A). The CTSL-CsA complex showed two well-defined large and strong energy minima basins, revealing a gradual conformational transition towards a more stable state (Figure 9B). The CTSL-phenytoin complex on the other hand is characterized by a large population shift towards a small, single-well energy basin, and a reversed population shift relative to the apo CTSL system indicating global conformational switch (Figure 9C). The CTSL-paclitaxel complex also depicted a reversed population shift with a large number of energy minima basins (Figure 9D). This indicates that the drugs induce diverse ensembles of flexible conformations during the 100 ns simulation. Thus, compared to apo CTSL free energy surfaces, there is a considerable population shift in all the CTSL-drug complex systems, suggesting that these drugs strongly modulate CTSL protein conformations, and thus could regulate the function of the protein.

To further examine the effect of drugs binding on secondary structure changes of CTSL, the time evolution of the secondary structure profiles during the simulation was monitored through DSSP and shown in Supporting information Figure S3. In the case of CTSL-drug complexes, no overall significant structural changes were observed. However, in case of CTSL-CsA complex, minor secondary structures like bridge and bends between H3 and H4 were converted to somewhat less prominent sheet structure indicating the structural stabilization in this complex. Overall, DSSP analysis indicates the minimal secondary structure changes in case of CTSL-drug complexes suggesting the strong and stable binding of drugs to CTSL.

The molecular docking and MD results thus showed strong and stable binding of the dugs CsA, phenytoin and paclitaxel to CTSL and thus could be considered as a potential therapeutic agent against the neurological comorbidity present in COVID-19 infection.

Very recently, we have reported CsA as candidate drug that binds to the host proteases, TMPRSS2, and cathepsin B/L and can inhibit the SARS-CoV-2 entry (Prasad et al., 2021b). Many other studies also reported CsA as a potential therapeutic drug in COVID-19 (Cour et al., 2020; Molyvdas and Matalon, 2020).

However, the management of COVID-19 in patients with different neurological comorbidities should be with more caution as the drug-drug

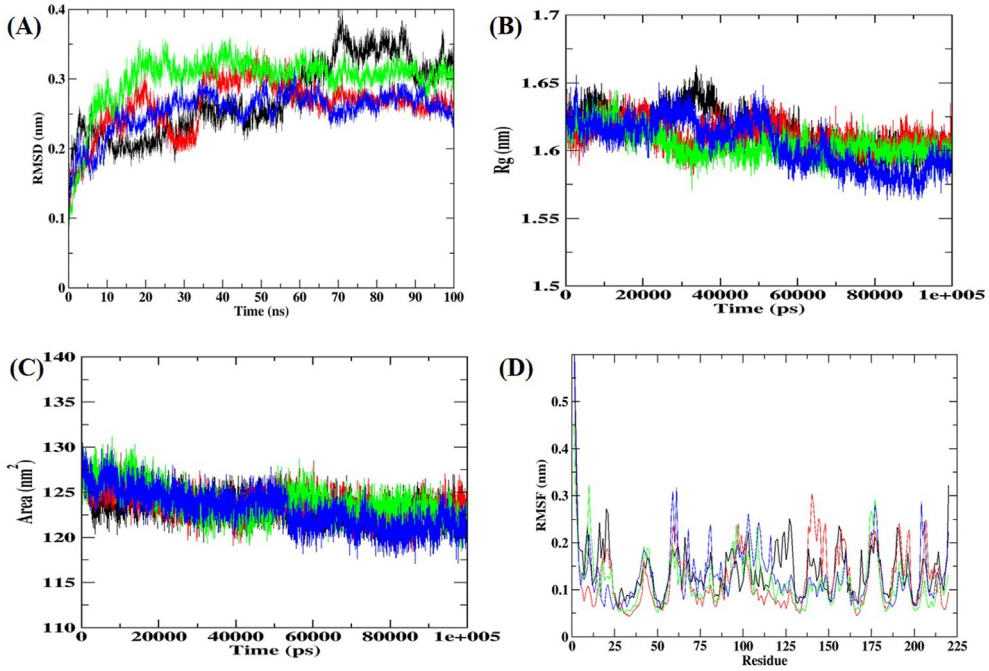

Figure 7. Molecular dynamics (MD) simulations result of CTSL-drug complexes during 100 ns at 300 K. (A) RMSD of the Cα backbone, (B) *Rg*, (C) SASA, and (D) RMSF of CTSL residues. In all panels the color code is-apo CTSL (black), CTSL-CsA (green), CTSL-phenytoin (blue), and CTSL-paclitaxel (red).

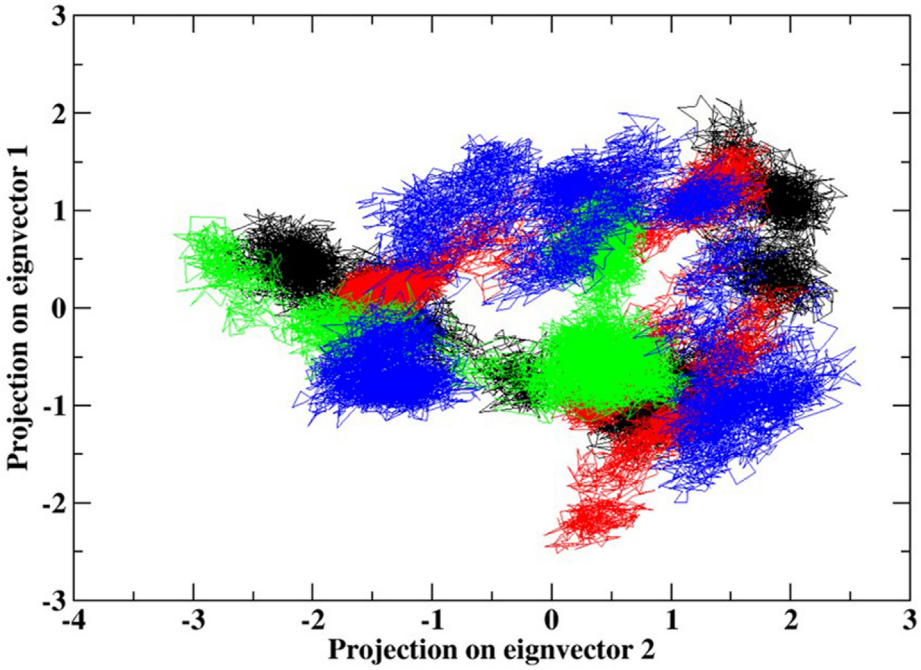

Figure 8. Principal component analysis (PCA) of CTSL-drug complexes during 100 ns MD simulation. Projection of the motion of the CTSL and CTSL-drug complexes in phase space along the PC1 and PC2.

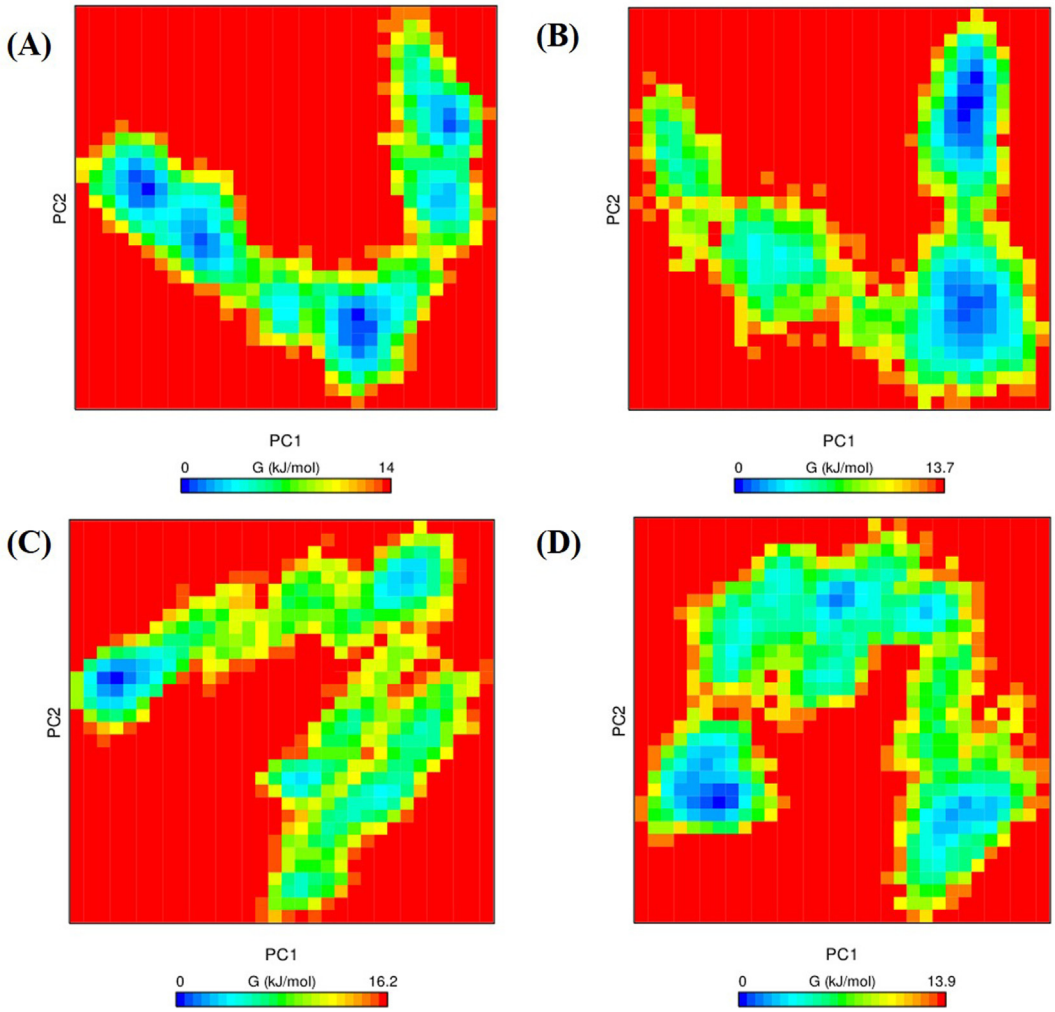

Figure 9. The free-energy landscape (FEL) of the simulated apo CTSL and CTSL-drug complexes based on PC1 and PC2. (A) apo CTSL, (B) CTSL-CsA, (C) CTSL-phenytoin, and (D) CTSL-paclitaxel. The color bar represents the free energy value according to kcal mol^{-1}.

interactions could pose significant challenges and thus may require adjustment to these drugs.

4. Conclusion

Lysosomal cathepsin proteases are involved in several brain disorders that occur at different developmental stages including brain injuries, lysosomal storage diseases, neurodegeneration, and many others. The elevation of cathepsins (Cathepsin B/L) has been previously demonstrated in brain disorders. Moreover, the pathophysiological hallmark of COVID-19 is the severe inflammation and cytokine storm, which explains the dysregulation of cathepsins. Based on our network analysis, we suggest that cathepsins B/L is an important marker of different neurological symptoms related to COVID-19, and targeting them will improve the clinical outcomes. We find potential therapies among different repurposable drugs that bind to the cathepsins and thus could block SARS- CoV-2 entry into host cells as well as alleviate the COVID-19 associated neurological complications.

Declarations

Author contribution statement

Kartikay Prasad: Performed the experiments; Analyzed and interpreted the data.

Shahzaib Ahamad: Performed the experiments; Analyzed and interpreted the data; Wrote the paper.

Dinesh Gupta: Contributed reagents, materials, analysis tools or data; Wrote the paper.

Vijay Kumar: Conceived and designed the experiments; Analyzed and interpreted the data; Contributed reagents, materials, analysis tools or data; Wrote the paper.

Funding statement

Shahzaib Ahamad was supported by the financial assistance from Indian Council of Medical Research, India. (2019–6039 File No. ISRM/11(83)/2019). Dinesh Gupta was supported by the Department of Biotechnology (Grant No. BT/BI/04/001/2018), Government of India.

Data availability statement

Data included in article/supplementary material/referenced in article.

Declaration of interests statement

The authors declare no conflict of interest.

Additional information

Supplementary content related to this article has been published online at https://doi.org/10.1016/j.heliyon.2021.e08089.

Acknowledgments

K.P., and V.K sincerely thank the Amity University, Noida for providing facilities.

References

Abdi, H., Williams, L.J., 2010. Principal component analysis. Wiley Interdis. Rev.: Comput. Stat. 2, 433–459.

Amberger, J.S., Bocchini, C.A., Scott, A.F., Hamosh, A., 2019. OMIM. org: leveraging knowledge across phenotype–gene relationships. Nucleic Acids Res. 47, D1038–D1043.

Berk, H., Henk, B., C, B.H.J., M, F.J.G.E., 1997. LINCS: a linear constraint solver for molecular simulations. J. Comput. Chem. 18, 1463–1472.

Berman, H.M., Westbrook, J., Feng, Z., Gilliland, G., Bhat, T.N., Weissig, H., Shindyalov, I.N., Bourne, P.E., 2000. The protein data bank. Nucleic Acids Res. 28, 235–242.

Bhimaneni, S.P., Verma, A., Kumar, A., 2021. Pathogenesis of COVID-19. COVID-19: Current Challenges and Future Perspectives. Bentham Science Publishers Ltd, pp. 27–34.

Cotto, K.C., Wagner, A.H., Feng, Y.-Y., Kiwala, S., Coffman, A.C., Spies, G., Wollam, A., Spies, N.C., Griffith, O.L., Griffith, M., 2018. DGIdb 3.0: a redesign and expansion of the drug–gene interaction database. Nucleic Acids Res. 46, D1068–D1073.

Cour, M., Ovize, M., Argaud, L., 2020. Cyclosporine A: a valid candidate to treat COVID-19 patients with acute respiratory failure? Crit. Care 24, 276.

Davis, A.P., Grondin, C.J., Johnson, R.J., Sciaky, D., McMorran, R., Wiegers, J., Wiegers, T.C., Mattingly, C.J., 2019. The comparative toxicogenomics database: update 2019. Nucleic Acids Res. 47, D948–D954.

Ellul, M.A., Benjamin, L., Singh, B., Lant, S., Michael, B.D., Easton, A., Kneen, R., Defres, S., Sejvar, J., Solomon, T., 2020. Neurological associations of COVID-19. Lancet Neurol.

Filatov, A., Sharma, P., Hindi, F., Espinosa, P.S., 2020. Neurological complications of coronavirus disease (COVID-19): encephalopathy. Cureus 12.

Gordon, J.C., Myers, J.B., Folta, T., Shoja, V., Heath, L.S., Onufriev, A., 2005. H++: a server for estimating p K as and adding missing hydrogens to macromolecules. Nucleic Acids Res. 33, W368–W371.

Gordon, D.E., Jang, G.M., Bouhaddou, M., Xu, J., Obernier, K., White, K.M., O'Meara, M.J., Rezelj, V.V., Guo, J.Z., Swaney, D.L., Tummino, T.A., Huttenhain, R., Kaake, R.M., Richards, A.L., Tutuncuoglu, B., Foussard, H., Batra, J., Haas, K., Modak, M., Kim, M., Haas, P., Polacco, B.J., Braberg, H., Fabius, J.M., Eckhardt, M., Soucheray, M., Bennett, M.J., Cakir, M., McGregor, M.J., Li, Q., Meyer, B., Roesch, F., Vallet, T., Mac Kain, A., Miorin, L., Moreno, E., Naing, Z.Z.C., Zhou, Y., Peng, S., Shi, Y., Zhang, Z., Shen, W., Kirby, I.T., Melnyk, J.E., Chorba, J.S., Lou, K., Dai, S.A., Barrio-Hernandez, I., Memon, D., Hernandez-Armenta, C., Lyu, J., Mathy, C.J.P., Perica, T., Pilla, K.B., Ganesan, S.J., Saltzberg, D.J., Rakesh, R., Liu, X., Rosenthal, S.B., Calviello, L., Venkataramanan, S., Liboy-Lugo, J., Lin, Y., Huang, X.P., Liu, Y., Wankowicz, S.A., Bohn, M., Safari, M., Ugur, F.S., Koh, C., Savar, N.S., Tran, Q.D., Shengjuler, D., Fletcher, S.J., O'Neal, M.C., Cai, Y., Chang, J.C.J., Broadhurst, D.J., Klippsten, S., Sharp, P.P., Wenzell, N.A., Kuzuoglu-Ozturk, D., Wang, H.Y., Trenker, R., Young, J.M., Cavero, D.A., Hiatt, J., Roth, T.L., Rathore, U., Subramanian, A., Noack, J., Hubert, M., Stroud, R.M., Frankel, A.D., Rosenberg, O.S., Verba, K.A., Agard, D.A., Ott, M., Emerman, M., Jura, N., et al., 2020. A SARS-CoV-2 protein interaction map reveals targets for drug repurposing. Nature 583, 459–468.

Gu, J., Gong, E., Zhang, B., Zheng, J., Gao, Z., Zhong, Y., Zou, W., Zhan, J., Wang, S., Xie, Z., Zhuang, H., Wu, B., Zhong, H., Shao, H., Fang, W., Gao, D., Pei, F., Li, X., He, Z., Xu, D., Shi, X., Anderson, V.M., Leong, A.S., 2005. Multiple organ infection and the pathogenesis of SARS. J. Exp. Med. 202, 415–424.

Guex, N., Peitsch, M.C., 1997. SWISS-MODEL and the Swiss-Pdb Viewer: an environment for comparative protein modeling. Electrophoresis 18, 2714–2723.

Gupta, M., Sharma, R., Kumar, A., 2018. Docking techniques in pharmacology: how much promising? Comput. Biol. Chem. 76, 210–217.

Gupta, A., Madhavan, M.V., Sehgal, K., Nair, N., Mahajan, S., Sehrawat, T.S., Bikdeli, B., Ahluwalia, N., Ausiello, J.C., Wan, E.Y., Freedberg, D.E., Kirtane, A.J., Parikh, S.A., Maurer, M.S., Nordvig, A.S., Accili, D., Bathon, J.M., Mohan, S., Bauer, K.A., Leon, M.B., Krumholz, H.M., Uriel, N., Mehra, M.R., Elkind, M.S.V., Stone, G.W., Schwartz, A., Ho, D.D., Bilezikian, J.P., Landry, D.W., 2020a. Extrapulmonary manifestations of COVID-19. Nat. Med. 26, 1017–1032.

Gupta, M., Sharma, R., Kumar, A., 2020b. Docking techniques in toxicology: an overview. Curr. Bioinf. 15, 600–610.

Hoffmann, M., Kleine-Weber, H., Schroeder, S., Kruger, N., Herrler, T., Erichsen, S., Schiergens, T.S., Herrler, G., Wu, N.H., Nitsche, A., Muller, M.A., Drosten, C., Pohlmann, S., 2020. SARS-CoV-2 cell entry depends on ACE2 and TMPRSS2 and is blocked by a clinically proven protease inhibitor. Cell 181, 271–280 e8.

Hook, V., Yoon, M., Mosier, C., Ito, G., Podvin, S., Head, B.P., Rissman, R., O'Donoghue, A.J., Hook, G., 2020. Cathepsin B in neurodegeneration of Alzheimer's disease, traumatic brain injury, and related brain disorders. Biochim. Biophys. Acta Protein Proteonomics 1868, 140428.

Hung, E.C., Chim, S.S., Chan, P.K., Tong, Y.K., Ng, E.K., Chiu, R.W., Leung, C.B., Sung, J.J., Tam, J.S., Lo, Y.M., 2003. Detection of SARS coronavirus RNA in the cerebrospinal fluid of a patient with severe acute respiratory syndrome. Clin. Chem. 49, 2108–2109.

Joung, I.S., Cheatham 3rd, T.E., 2008. Determination of alkali and halide monovalent ion parameters for use in explicitly solvated biomolecular simulations. J. Phys. Chem. B 112, 9020–9041.

Kabsch, W., Sander, C., 1983. Dictionary of protein secondary structure: pattern recognition of hydrogen-bonded and geometrical features. Biopolymers 22, 2577–2637.

Kanberg, N., Ashton, N.J., Andersson, L.M., Yilmaz, A., Lindh, M., Nilsson, S., Price, R.W., Blennow, K., Zetterberg, H., Gisslen, M., 2020. Neurochemical evidence of astrocytic and neuronal injury commonly found in COVID-19. Neurology 95 (12), e1754–e1759.

Khatoon, F., Prasad, K., Kumar, V., 2020. Neurological manifestations of COVID-19: available evidences and a new paradigm to understand the complications. J. Neurovirol. 1–2.

Khatoon, F., Prasad, K., Kumar, V., 2021. COVID-19 associated nervous system manifestations [published online ahead of print, 2021 Jul 9]. Sleep Med. S1389-9457(21)00387-7.

Kim, S., Chen, J., Cheng, T., Gindulyte, A., He, J., He, S., Li, Q., Shoemaker, B.A., Thiessen, P.A., Yu, B., 2019. PubChem 2019 update: improved access to chemical data. Nucleic Acids Res. 47, D1102–D1109.
Kim, S., Chen, J., Cheng, T., Gindulyte, A., He, J., He, S., Li, Q., Shoemaker, B.A., Thiessen, P.A., Yu, B., 2021. PubChem in 2021: new data content and improved web interfaces. Nucleic Acids Res. 49, D1388–D1395.
Kuhn, M., von Mering, C., Campillos, M., Jensen, L.J., Bork, P., 2007. STITCH: interaction networks of chemicals and proteins. Nucleic Acids Res. 36, D684–D688.
Kumar, V., Prakash, A., Lynn, A.M., 2018. Alterations in local stability and dynamics of A4V SOD1 in the presence of trifluoroethanol. Biopolymers 109, e23102.
Kumar, V., Pandey, P., Idrees, D., Prakash, A., Lynn, A.M., 2019. Delineating the effect of mutations on the conformational dynamics of N-terminal domain of TDP-43. Biophys. Chem. 250, 106174.
Lee, J., Cheng, X., Swails, J.M., Yeom, M.S., Eastman, P.K., Lemkul, J.A., Wei, S., Buckner, J., Jeong, J.C., Qi, Y., 2016. CHARMM-GUI input generator for NAMD, GROMACS, AMBER, OpenMM, and CHARMM/OpenMM simulations using the CHARMM36 additive force field. J. Chem. Theor. Comput. 12, 405–413.
Leonardi, M., Padovani, A., McArthur, J.C., 2020. Neurological manifestations associated with COVID-19: a review and a call for action. J. Neurol. 267, 1573–1576.
Li, Q., Guan, X., Wu, P., Wang, X., Zhou, L., Tong, Y., Ren, R., Leung, K.S.M., Lau, E.H.Y., Wong, J.Y., Xing, X., Xiang, N., Wu, Y., Li, C., Chen, Q., Li, D., Liu, T., Zhao, J., Liu, M., Tu, W., Chen, C., Jin, L., Yang, R., Wang, Q., Zhou, S., Wang, R., Liu, H., Luo, Y., Liu, Y., Shao, G., Li, H., Tao, Z., Yang, Y., Deng, Z., Liu, B., Ma, Z., Zhang, Y., Shi, G., Lam, T.T.Y., Wu, J.T., Gao, G.F., Cowling, B.J., Yang, B., Leung, G.M., Feng, Z., 2020. Early transmission dynamics in Wuhan, China, of novel coronavirus-infected pneumonia. N. Engl. J. Med. 382, 1199–1207.
Mao, L., Jin, H., Wang, M., Hu, Y., Chen, S., He, Q., Chang, J., Hong, C., Zhou, Y., Wang, D., Miao, X., Li, Y., Hu, B., 2020. Neurologic manifestations of hospitalized patients with coronavirus disease 2019 in Wuhan, China. JAMA Neurol 683–690.
McGibbon, R.T., Beauchamp, K.A., Harrigan, M.P., Klein, C., Swails, J.M., Hernandez, C.X., Schwantes, C.R., Wang, L.P., Lane, T.J., Pande, V.S., 2015. MDTraj: a modern open library for the analysis of molecular dynamics trajectories. Biophys. J. 109, 1528–1532.
Mehta, P., McAuley, D.F., Brown, M., Sanchez, E., Tattersall, R.S., Manson, J.J., 2020. COVID-19: consider cytokine storm syndromes and immunosuppression. Lancet 395, 1033–1034.
Millet, J.K., Whittaker, G.R., 2015. Host cell proteases: critical determinants of coronavirus tropism and pathogenesis. Virus Res. 202, 120–134.
Molyvdas, A., Matalon, S., 2020. Cyclosporine: an old weapon in the fight against coronaviruses. Eur. Respir. J. 56.
Morris, G.M., Huey, R., Lindstrom, W., Sanner, M.F., Belew, R.K., Goodsell, D.S., Olson, A.J., 2009. AutoDock4 and AutoDockTools4: automated docking with selective receptor flexibility. J. Comput. Chem. 30, 2785–2791.
Ou, X., Liu, Y., Lei, X., Li, P., Mi, D., Ren, L., Guo, L., Guo, R., Chen, T., Hu, J., Xiang, Z., Mu, Z., Chen, X., Chen, J., Hu, K., Jin, Q., Wang, J., Qian, Z., 2020. Characterization of spike glycoprotein of SARS-CoV-2 on virus entry and its immune cross-reactivity with SARS-CoV. Nat. Commun. 11, 1620.
Pandey, P., Prasad, K., Prakash, A., Kumar, V., 2020. Insights into the biased activity of dextromethorphan and haloperidol towards SARS-CoV-2 NSP6: in silico binding mechanistic analysis. J. Mol. Med. (Berl.) 98, 1659–1673.
Paniz-Mondolfi, A., Bryce, C., Grimes, Z., Gordon, R.E., Reidy, J., Lednicky, J., Sordillo, E.M., Fowkes, M., 2020. Central nervous system involvement by severe acute respiratory syndrome coronavirus-2 (SARS-CoV-2). J. Med. Virol. 92, 699–702.
Paoloni-Giacobino, A., Chen, H., Peitsch, M.C., Rossier, C., Antonarakis, S.E., 1997. Cloning of the TMPRSS2 gene, which encodes a novel serine protease with transmembrane, LDLRA, and SRCR domains and maps to 21q22.3. Genomics 44, 309–320.
Podvin, S., Wojnicz, A., Hook, V., 2018. Human brain gene expression profiles of the cathepsin V and cathepsin L cysteine proteases, with the PC1/3 and PC2 serine proteases, involved in neuropeptide production. Heliyon 4, e00673.
Poyiadji, N., Shahin, G., Noujaim, D., Stone, M., Patel, S., Griffith, B., 2020. COVID-19–associated acute hemorrhagic necrotizing encephalopathy: CT and MRI features. Radiology 201187.
Prakash, A., Kumar, V., Banerjee, A., Lynn, A.M., Prasad, R., 2021. Structural heterogeneity in RNA recognition motif 2 (RRM2) of TAR DNA-binding protein 43 (TDP-43): clue to amyotrophic lateral sclerosis. J. Biomol. Struct. Dyn. 39, 357–367.
Prasad, K., Khatoon, F., Rashid, S., Ali, N., AlAsmari, A.F., Ahmed, M.Z., Alqahtani, A.S., Alqahtani, M.S., Kumar, V., 2020. Targeting hub genes and pathways of innate immune response in COVID-19: a network biology perspective. Int. J. Biol. Macromol. 163, 1–8.
Prasad, K., AlOmar, S.Y., Alqahtani, S.A.M., Malik, M.Z., Kumar, V., 2021a. Brain disease network analysis to elucidate the neurological manifestations of COVID-19. Mol. Neurobiol. 58 (5), 1875–1893.
Prasad, K., Ahamad, S., Kanipakam, H., Gupta, D., Kumar, V., 2021b. Simultaneous inhibition of SARS-CoV-2 entry pathways by cyclosporine. ACS Chem. Neurosci. 12, 930–944.
Price, D.J., Brooks III, C.L., 2004. A modified TIP3P water potential for simulation with Ewald summation. J. Chem. Phys. 121, 10096–10103.
Rappaport, N., Twik, M., Plaschkes, I., Nudel, R., Iny Stein, T., Levitt, J., Gershoni, M., Morrey, C.P., Safran, M., Lancet, D., 2017. MalaCards: an amalgamated human disease compendium with diverse clinical and genetic annotation and structured search. Nucleic Acids Res. 45, D877–D887.
Robinson, Emma L., Alkass, Kanar, Bergmann, Olaf, Janet, J., Maguire, H., Roderick, Llewelyn, Davenport, A.P., 2020. Genes encoding ACE2, TMPRSS2 and related proteins mediating SARS-CoV-2 viral entry are upregulated with age in human cardiomyocytes. BioRxiv.
Sang, P., Wang, L., Cao, J., 2017. Parametric functional principal component analysis. Biometrics 73, 802–810.
Sau, S., Kumar, A., 2021. COVID-19 Altered Immune Signalling Pathways: COVID-19: Current Challenges and Future Perspectives. Bentham Science Publishers Ltd.
Schattelkopf, A.W., Van Aalten, D.M.F., 2004. PRODRG: a tool for high-throughput crystallography of proteinâ€“ligand complexes. Acta Crystallogr. Sect. D Biol. Crystallogr. 60, 1355–1363.
Shannon, P., Markiel, A., Ozier, O., Baliga, N.S., Wang, J.T., Ramage, D., Amin, N., Schwikowski, B., Ideker, T., 2003. Cytoscape: a software environment for integrated models of biomolecular interaction networks. Genome Res. 13, 2498–2504.
Stelzer, G., Rosen, N., Plaschkes, I., Zimmerman, S., Twik, M., Fishilevich, S., Stein, T.I., Nudel, R., Lieder, I., Mazor, Y., 2016. The GeneCards suite: from gene data mining to disease genome sequence analyses. Curr Prot Bioinform 54, 1.30. 1-1.30. 33.
Toscano, G., Palmerini, F., Ravaglia, S., Ruiz, L., Invernizzi, P., Cuzzoni, M.G., Franciotta, D., Baldanti, F., Daturi, R., Postorino, P., Cavallini, A., Micieli, G., 2020. Guillain-barre syndrome associated with SARS-CoV-2. N. Engl. J. Med. 382, 2574–2576.
Trott, O., Olson, A.J., 2010. AutoDock Vina: improving the speed and accuracy of docking with a new scoring function, efficient optimization, and multithreading. J. Comput. Chem. 31, 455–461.
Vanommeslaeghe, K., Hatcher, E., Acharya, C., Kundu, S., Zhong, S., Shim, J., Darian, E., Guvench, O., Lopes, P., Vorobyov, I., 2010. CHARMM general force field: a force field for drug-like molecules compatible with the CHARMM all-atom additive biological force fields. J. Comput. Chem. 31, 671–690.
Wang, H., Yang, P., Liu, K., Guo, F., Zhang, Y., Zhang, G., Jiang, C., 2008. SARS coronavirus entry into host cells through a novel clathrin- and caveolae-independent endocytic pathway. Cell Res. 18, 290–301.
Wang, H., Nakamura, H., Fukuda, I., 2016. A critical appraisal of the zero-multipole method: structural, thermodynamic, dielectric, and dynamical properties of a water system. J. Chem. Phys. 144, 114503.
Wang, K., Chen, W., Zhou, Y.-S., 2020. SARSCoV-2 invades host cells via a novel route: CD147-spike protein. bioRxiv.
Wishart, D.S., Knox, C., Guo, A.C., Cheng, D., Shrivastava, S., Tzur, D., Gautam, B., Hassanali, M., 2008. DrugBank: a knowledgebase for drugs, drug actions and drug targets. Nucleic Acids Res. 36, D901–D906.
Wishart, D.S., Feunang, Y.D., Guo, A.C., Lo, E.J., Marcu, A., Grant, J.R., Sajed, T., Johnson, D., Li, C., Sayeeda, Z., 2018. DrugBank 5.0: a major update to the DrugBank database for 2018. Nucleic Acids Res. 46, D1074–D1082.
Xu, J., Zhong, S., Liu, J., Li, L., Li, Y., Wu, X., Li, Z., Deng, P., Zhang, J., Zhong, N., Ding, Y., Jiang, Y., 2005. Detection of severe acute respiratory syndrome coronavirus in the brain: potential role of the chemokine mig in pathogenesis. Clin. Infect. Dis. 41, 1089–1096.
Yin, Junping, Kasper, Brigitte, Petersen, Frank, Yu, X., 2020. Expression of ACE2, TMPRSS2 and CTSL in human airway epithelial cells under physiological and pathological conditions: implications for SARS-CoV-2 infection. BioRxiv.
Zhou, Y., Vedantham, P., Lu, K., Agudelo, J., Carrion Jr., R., Nunneley, J.W., Barnard, D., Pohlmann, S., McKerrow, J.H., Renslo, A.R., Simmons, G., 2015. Protease inhibitors targeting coronavirus and filovirus entry. Antivir. Res. 116, 76–84.
Zhou, L., Zhang, M., Wang, J., Gao, J., 2020a. Sars-Cov-2: underestimated damage to nervous system. Trav. Med. Infect. Dis. 101642.
Zhou, P., Yang, X.L., Wang, X.G., Hu, B., Zhang, L., Zhang, W., Si, H.R., Zhu, Y., Li, B., Huang, C.L., Chen, H.D., Chen, J., Luo, Y., Guo, H., Jiang, R.D., Liu, M.Q., Chen, Y., Shen, X.R., Wang, X., Zheng, X.S., Zhao, K., Chen, Q.J., Deng, F., Liu, L.L., Yan, B., Zhan, F.X., Wang, Y.Y., Xiao, G.F., Shi, Z.L., 2020b. A pneumonia outbreak associated with a new coronavirus of probable bat origin. Nature 579, 270–273.
Zubair, A.S., McAlpine, L.S., Gardin, T., Farhadian, S., Kuruvilla, D.E., Spudich, S., 2020. Neuropathogenesis and neurologic manifestations of the coronaviruses in the age of coronavirus disease 2019: a review. JAMA Neurol 77 (8), 1018–1027.
Zuberi, K., Franz, M., Rodriguez, H., Montojo, J., Lopes, C.T., Bader, G.D., Morris, Q., 2013. GeneMANIA prediction server 2013 update. Nucleic Acids Res. 41, W115–W122.